Earth and Planetary Science Letters 465 (2017) 134–144

Contents lists available at ScienceDirect

Earth and Planetary Science Letters

www.elsevier.com/locate/epsl

Spatial variations in cooling rate in the mantle section of the Samail ophiolite in Oman: Implications for formation of lithosphere at mid-ocean ridges

Nick Dygert[a,*], Peter B. Kelemen[b], Yan Liang[c]

[a] Department of Geological Sciences, University of Texas at Austin, Austin, TX 78712, United States
[b] Department of Earth and Environmental Sciences, Columbia University, Lamont Doherty Earth Observatory, Palisades, NY 10964, United States
[c] Department of Earth, Environmental and Planetary Sciences, Brown University, Providence, RI 02912, United States

ARTICLE INFO

Article history:
Received 12 July 2016
Received in revised form 20 February 2017
Accepted 22 February 2017
Available online xxxx
Editor: M. Bickle

Keywords:
Mantle
REE
thermometry
Oman ophiolite
closure temperature
geospeedometry

ABSTRACT

To understand how the mantle cools beneath mid-ocean ridge spreading centers, we applied a REE-in-two-pyroxene thermometer and major element thermometers to peridotites from the Wadi Tayin massif in the southern part of the Samail ophiolite in the Sultanate of Oman, which represent more than 10 km of structural depth beneath the paleo-Moho. Closure temperatures for REEs in pyroxenes deduced from the REE-in-two-pyroxene thermometer (T_{REE}) decrease smoothly and systematically with depth in the section, from >1300 °C near the crust to <1100 °C near the metamorphic sole, consistent with previously observed, similar variations in mineral thermometers with lower cooling temperatures. Estimated cooling rates decrease from ∼0.3 °C/y just below the crust–mantle transition zone (MTZ) to $\sim 10^{-3}$ °C/y at a depth of six km below the MTZ. Cooling rates derived from Ca-in-olivine thermometry also decrease moving deeper into the section. These variations in cooling rate are most consistent with conductive cooling of the mantle beneath a cold overlying crust. In turn, this suggests that hydrothermal circulation extended to the MTZ near the axis of the fast-spreading ridge where the igneous crust of the Samail ophiolite formed. These observations are consistent with the Sheeted Sills model for accretion of lower oceanic crust, and with previous work demonstrating very rapid cooling rates in the crust of the Wadi Tayin massif. Our observations, combined with previous results, suggest that efficient hydrothermal circulation beneath fast spreading centers cools the uppermost mantle from magmatic temperatures to <1000 °C as quickly as tectonic exhumation at amagmatic spreading centers. In contrast, thermometers sensitive to cooling over lower temperature intervals indicate that the Wadi Tayin peridotites cooled more slowly than tectonically exhumed peridotites sampled near the seafloor along mid-ocean ridges. Hydrothermal cooling of the crust may have waned, so that the crust–mantle package cooled more slowly, whereas rapid cooling of abyssal peridotites during tectonic exhumation continued to seafloor temperatures.

1. Introduction

Geothermometers are widely used to investigate the thermal history of mafic and ultramafic rocks. They utilize the temperature dependent solubility or partitioning of a component among phases in a mineral assemblage, allowing temperatures to be calculated from measured mineral compositions. Geothermometers are calibrated experimentally or with well-equilibrated natural samples, and depending on the thermometer, take advantage of temperature dependent major element (e.g., Boyd, 1973; Brey and Köhler, 1990; Nickel and Green, 1985; Putirka, 2008; Wells, 1977; Witt-Eickschen and Seck, 1991; Wood and Banno, 1973) and/or trace element exchange reactions (Eggins et al., 1998; Lee et al., 2007; Liang et al., 2013; Seitz et al., 1999; Sun and Liang, 2015; Witt-Eickschen and O'Neill, 2005).

The physical meaning of a temperature derived from the application of a geothermometer to a natural sample depends on its thermal history. In cases where the sample is maintained at constant pressure and temperate conditions and then rapidly exhumed or erupted, any well calibrated geothermometer should give a temperature reflecting the condition of equilibration in agreement with other thermometers (e.g., Liang et al., 2013; Smith, 2013; Witt-Eickschen and Seck, 1991). No kinetic information is preserved in such samples. In contrast, if the sample cools sufficiently

* Corresponding author at: Jackson School of Geosciences, University of Texas at Austin, 2275 Speedway Stop C9000, Austin, TX 78712.
E-mail address: ndygert@jsg.utexas.edu (N. Dygert).

http://dx.doi.org/10.1016/j.epsl.2017.02.038

slowly to allow appreciable diffusive reequilibration to occur during cooling, geothermometers will give a range of temperatures. All will record higher temperatures for faster cooling rates, providing the basis for "geospeedometry" (e.g., Dodson, 1973; Lasaga, 1983; Ozawa, 1984), a powerful tool that has been widely used to study the thermal history of crust and mantle formed at oceanic spreading ridges (e.g., Coogan et al., 2002, 2005a, 2007a, 2007b; Dygert and Liang, 2015; Faak et al., 2015; Faak and Gillis, 2016; VanTongeren et al., 2008). In addition, the temperature recorded by a given thermometer will depend on the effective diffusion rates of the components used to calibrate the thermometer. Thermometers based on slowly diffusing elements record higher temperatures than those based on faster diffusing elements (e.g., for peridotites, Dygert and Liang, 2015; Hanghøj et al., 2010; Liang et al., 2013; Müntener et al., 2010; Yao and Liang, 2015).

In this work we will discuss temperatures from three types of thermometers. (1) The REE-in-two-pyroxene thermometer of Liang et al. (2013), which utilizes the composition-dependent temperature sensitivity of exchange of trivalent REEs + Y between orthopyroxene (opx) and clinopyroxene (cpx). (2) Two-pyroxene solvus thermometers (e.g., Brey and Köhler, 1990; Lindsley, 1983; Lindsley and Anderson, 1983; Wells, 1977), which parameterize temperature sensitive "transfer of the enstatite component between coexisting ortho- and clinopyroxene" around the solvus (Brey and Köhler, 1990). In reality, this exchange reaction is more complicated as unmixing of solid solutions during cooling involves coupled diffusion of several major elements (e.g., Ca, Mg and Si), and net growth of one phase at the expense of another. (3) Cation exchange thermometers, which parameterize the temperature sensitivity of exchange of major elements between two phases (e.g., Fabriès, 1979; Köhler and Brey, 1990). For samples that cooled slowly, thermometers based on exchange of trivalent elements (e.g., REEs, Al) give temperatures tens to hundreds of degrees higher than two-pyroxene solvus thermometers, which in turn give higher temperatures than divalent cation exchange thermometers (e.g., D'Errico et al., 2016; Dygert and Liang, 2015; Liang et al., 2013; Marchesi et al., 2016; Müntener et al., 2010; Sun and Liang, 2015; Wang et al., 2015; Witt-Eickschen and Seck, 1991). These differences in temperature can be attributed to slower diffusion of trivalent elements compared to divalent elements (e.g., Chakraborty, 2010; Cherniak and Dimanov, 2010 and references therein), and the slower diffusion of multivalent mineral components compared to interdiffusion of isovalent cations.

As a general rule, the larger the difference between the temperatures given by thermometers based on trivalent elements and solvus or cation exchange thermometers, the slower the average cooling rate for the sample. Thermometers based on trivalent cation exchange may reflect cooling rates in high temperature intervals along the cooling path; solvus thermometers may reflect cooling rates in intermediate temperature intervals along the cooling path. Divalent cation exchange thermometers are sensitive to lower temperature cooling intervals, and among themselves, are sensitive to cooling at different temperatures, with thermometers based on the fastest diffusing cations reflecting cooling over the lowest temperature intervals.

In a recent study, Dygert and Liang (2015) applied the REE-in-two-pyroxene thermometer of Liang et al. (2013) and several solvus thermometers to abyssal peridotites and peridotites sampled from the mantle section of ophiolites. Some ophiolites cooled more slowly than abyssal peridotites. This was expected, as abyssal peridotites are dredged from mantle exposures that were tectonically exhumed along transform faults and detachment faults in less than a million years, while ophiolites have crustal sections that generally act as insulating barriers for underlying mantle peridotites for many millions of years. In contrast, peridotites from the northern Samail ophiolite appear to have cooled as quickly as the abyssal peridotites based on REE thermometry. This is surprising as the Samail ophiolite has a thick (5–7 km) crustal section and probably formed at a fast-spreading center (e.g., Nicolas, 1989; Rioux et al., 2012, 2013, 2016; Tilton et al., 1981), suggesting that cooling of the mantle beneath mid-ocean ridges is independent of spreading rate and the presence or absence of crust, at least in the temperature interval from ~1300 to 1000 °C.

To investigate the thermal history of mantle peridotites beneath thick crustal sections, as compared to mantle peridotites that are tectonically exhumed along faults near mid-ocean ridges, we applied the REE-in-two-pyroxene thermometer (Liang et al., 2013) and conventional major element-based pyroxene solvus, olivine-cpx and olivine-spinel cation exchange thermometers (Brey and Köhler, 1990; Fabriès, 1979; Köhler and Brey, 1990; Putirka, 2008; Wells, 1977; Witt-Eickschen and Seck, 1991) to a suite of samples from the Wadi Tayin massif in the southern Samail ophiolite (Fig. 1), previously studied by Hanghøj et al. (2010). Corrected for structural depth beneath the paleo–Moho, assuming that there is a constant dip parallel to the crust–mantle transition, and that there are no faults that repeat or omit section, these samples represent more than 10 km of paleo-depth below the Moho, with continuous outcrop. Samples from this section can thus be used to investigate the dependence of cooling rate on depth beneath the crust.

Our focus on the Wadi Tayin massif was motivated by the observation of large gradients in major element thermometer temperatures across the mantle section, with higher temperatures in mantle samples near the base of the crust and lower temperatures deeper in the section (Fig. 2, also see Fig. 7 in Hanghøj et al., 2010). In addition, interpretation of closure temperatures for olivine-cpx Ca–Mg exchange indicates that the entire crustal section in the Wadi Tayin massif cooled very rapidly, with no systematic gradient in cooling rate with depth in the crust (VanTongeren et al., 2008).

The southern massifs of the Samail ophiolite show some geochemical characteristics indicative of a "subduction component" (e.g., Pearce et al., 1981 and recent reviews in MacLeod et al., 2013 and Rioux et al., 2016), but also record a fast rate of submarine, sea-floor spreading (Rioux et al., 2012, 2013; Tilton et al., 1981). The massifs have a well-developed, gabbroic lower crust underlying sheeted dikes and pillow basalts, with mid-ocean ridge basalt (MORB)-like parental magmas and trace element chemistry, and they have mantle composition similar to abyssal peridotites (e.g., Braun, 2004; Garrido et al., 2001; Godard et al., 2000; Hanghøj et al., 2010; Kelemen et al., 1995, 1997a, 1997b; Nicolas, 1989; Pallister and Knight, 1981). Thus, the southern massifs of the Samail ophiolite in Oman represent the ophiolites with the greatest affinities to crust formed at fast-spreading mid-ocean ridges. As a result, our study provides new insight into the processes that cool the mantle beneath present-day, fast-spreading mid-ocean ridges such as the East Pacific Rise.

2. Samples and mineral compositions

Here we report major element compositions from analyses of opx, cpx and olivine and trace element compositions of opx and cpx in eight peridotites from the OM94 traverse originally studied by Hanghøj et al. (2010) (Fig. 3, Supplementary Tables S1 and S2, Supplementary Figs. S2–S5). Analytical methods are described in the Electronic Supplement. The samples are depleted, plagioclase-free harzburgites. Pyroxene minor element concentrations plot at the depleted ends of the ophiolitic and abyssal peridotite fields (Figs. 3a, 3b, Supplementary Figs. S2, S3). Consistent with the depleted pyroxene compositions, bulk rock REE and other incompatible trace element characteristics in Wadi Tayin peridotites overlap the low end of the compositional range for abyssal peridotites (Fig. 3a in Hanghøj et al., 2010). Similarly, spinel Cr#s in

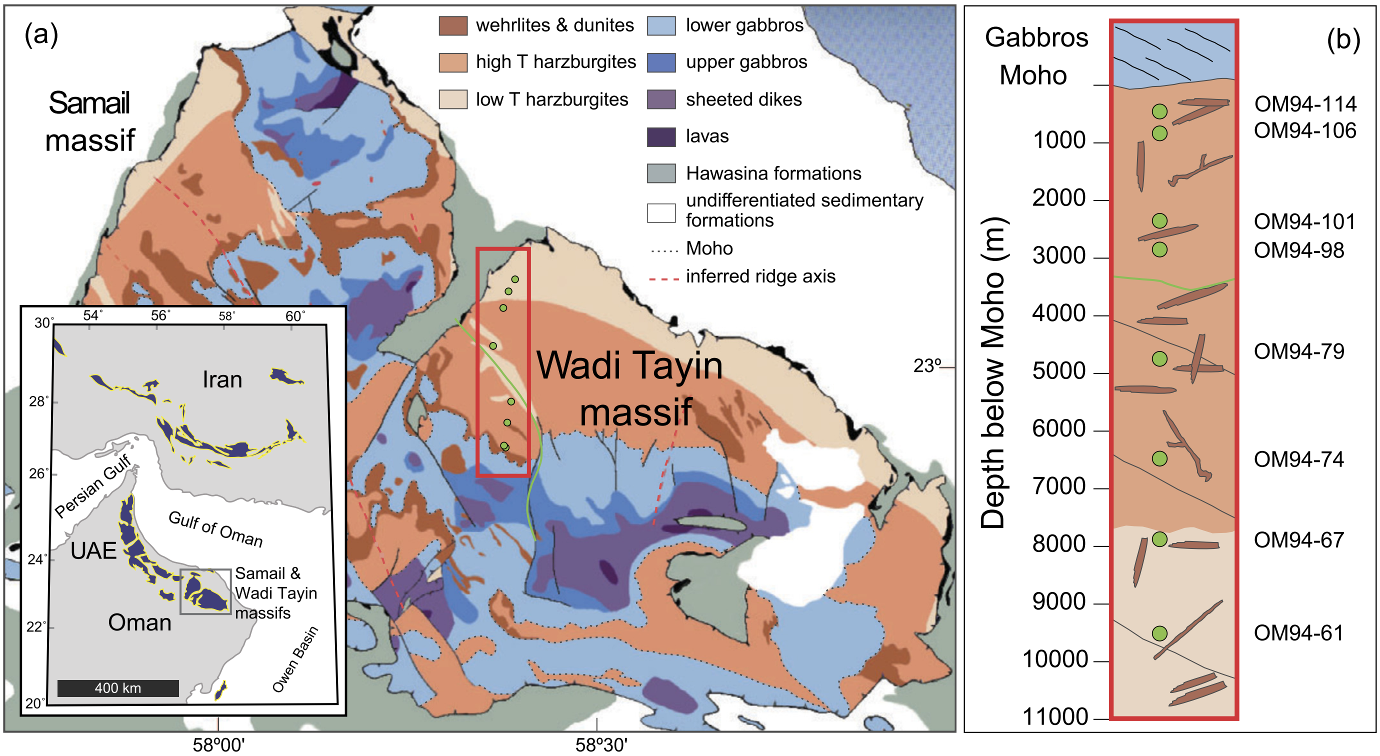

Fig. 1. (a) A geologic map of the Wadi Tayin massif, Samail ophiolite, modified from Hanghøj et al. (2010), and Nicolas et al. (2001). Inset shows the location of the massif in southern Oman. Approximate locations of our samples are shown by the green circles. The green line cutting across the sample area is the Makhibiyah shear zone, which is thought to have accommodated little or no relative motion between the adjacent blocks (Nicolas and Boudier, 2008). (b) The approximate depth of each sample beneath the crustal section, assuming that there is a constant dip parallel to the crust–mantle transition, and that no faults repeat or omit section. (For interpretation of the references to color in this figure legend, the reader is referred to the web version of this article.)

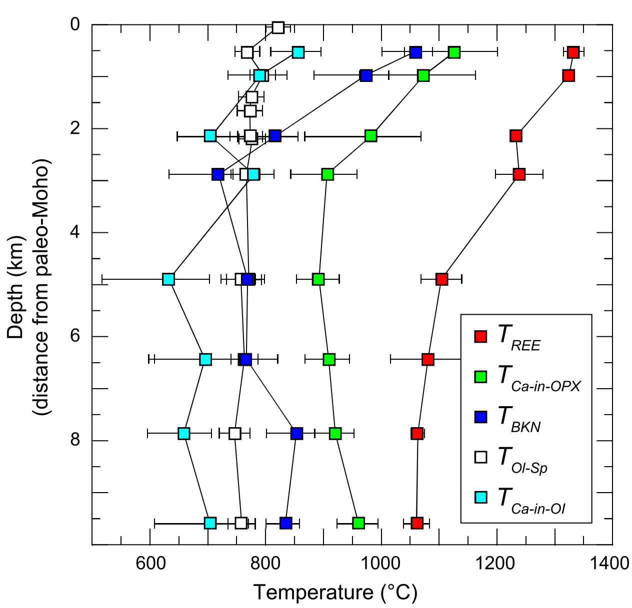

Fig. 2. T_{REE}, T_{BKN}, $T_{Ca\text{-}in\text{-}Opx}$, $T_{Ca\text{-}in\text{-}Ol}$, and $T_{Ol\text{-}Sp}$ plotted as a function of distance from the paleo-Moho for our OM94 samples. Note T_{REE}, T_{BKN}, $T_{Ca\text{-}in\text{-}Opx}$, and $T_{Ca\text{-}in\text{-}Ol}$ decrease moving deeper into the section. Aside from a slight decrease at the top of the section, $T_{Ol\text{-}Sp}$ exhibits little systematic variation with depth. T_{REE}, T_{BKN} and $T_{Ca\text{-}in\text{-}Opx}$ may reflect to high temperature cooling histories while $T_{Ol\text{-}Sp}$ and $T_{Ca\text{-}in\text{-}Ol}$ may reflect low temperature cooling histories. The sensitivity of a thermometer to cooling over a particular temperature interval depends on its formulation (see main text).

the Wadi Tayin and adjacent Samail massif mantle sections range from 35 to 73 (Cr# = 100 × molar Cr/(Cr + Al); Braun, 2004; Hanghøj et al., 2010; Koga et al., 2001; Korenaga and Kelemen, 1997), overlapping the high end of the range in depleted abyssal peridotites (maximum Cr# ∼ 60) and extending to slightly higher values (e.g., Dick and Bullen, 1984; updated compilation in Fig. 5 of Hanghøj et al., 2010). With the exception of one sample that has slightly elevated REE concentrations and may have experienced late-stage melt infiltration (OM94-114, Hanghøj et al., 2010), REEs in cpx overlap the low ends of the fields defined by abyssal peridotites and ophiolites (Fig. 3 in Kelemen et al., 1995). REE concentrations are generally higher in samples deep in the section, and lower close to the Moho, consistent with increasing extents of depletion with decreasing depth, due to decompression melting and melt extraction. This agrees with the previous observation that spinel Cr# in harzburgites increases upward from the base of the section toward the Moho (Hanghøj et al., 2010). Other major elements exhibit little systematic variation as a function of distance from the Moho (Supplementary Fig. S5). Overall, these observations suggest that the Wadi Tayin peridotites are residues of decompression melting beneath a spreading center similar to a fast-spreading mid-ocean ridge.

3. Temperatures and cooling rates

Temperatures obtained using the REE-in-two-pyroxene thermometer of Liang et al. (2013) and solvus and cation exchange thermometers developed by Brey and Köhler (1990), Köhler and Brey (1990), and Fabriès (1979) are plotted in Fig. 2 as a function of distance from the paleo-Moho. Brey and Köhler's Ca-in-opx thermometer ($T_{Ca\text{-}in\text{-}Opx}$) is based on the Ca content of opx along the solvus between two pyroxenes, and their two-pyroxene thermometer (T_{BKN}) parameterizes unmixing along the solidus to form cpx with different proportions of the diopside component. Köhler and Brey's Ca-in-olivine thermometer ($T_{Ca\text{-}in\text{-}Ol}$) is based on Ca–Mg exchange between olivine and clinopyroxene. The olivine-spinel thermometer (T_{Ol-Sp}) of Fabriès parameterizes Fe–Mg ex-

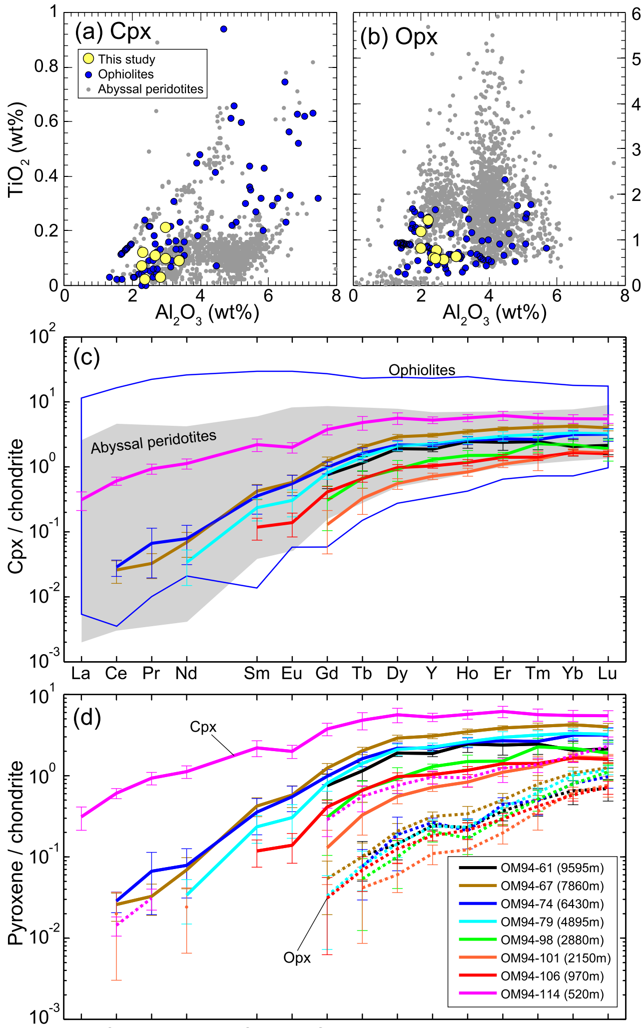

Fig. 3. Pyroxene compositions in OM94 samples compared to abyssal and ophiolitic peridotites. Abyssal peridotite data are from PetDB, and data for ophiolitic peridotites are from the compilation of Dygert and Liang (2015) (see caption to Fig. 4 for individual references). Incompatible minor elements are shown in (a) cpx and (b) opx. Note the OM94 samples plot with depleted abyssal and ophiolitic peridotites, suggesting high extents of partial melting. (c) Chondrite normalized REEs in cpx from ophiolites and abyssal peridotites. REE patterns and concentrations are similar to depleted abyssal peridotites, as also reflected in whole rock data for REEs and other incompatible trace elements (Hanghøj et al., 2010, Figs. 3 and 4). Concentrations of REEs in cpx generally increase moving deeper into the section, with the exception of OM94-114 which may have experienced a melt infiltration event (Hanghøj et al., 2010). (d) Chondrite normalized REE concentrations in cpx (solid lines) and opx (dotted lines). Error bars are 1σ standard deviations of replicate analyses.

change between the two minerals. For each sample, the thermometers give different temperatures, but the variation in T_{REE}, T_{BKN}, $T_{Ca\text{-}in\text{-}Opx}$, and $T_{Ca\text{-}in\text{-}Ol}$ is fairly well-correlated. For those thermometers, samples near the paleo-Moho have higher temperatures than samples deeper in the section, as previously shown for T_{BKN}, and $T_{Ca\text{-}in\text{-}Opx}$ by Hanghøj et al. (2010, see their Fig. 7). As shown in Fig. 2, T_{REE} exhibit a smooth and systematic decrease from >1300 °C near the crust to <1100 °C at the bottom of the section, while $T_{Ca\text{-}in\text{-}Opx}$ and T_{BKN} show slightly different patterns, with highest temperatures near the crust (T_{BKN} = 1060 °C, $T_{Ca\text{-}in\text{-}Opx}$ = 1127 °C), lowest temperatures in the middle of the section (T_{BKN} = 718 °C, $T_{Ca\text{-}in\text{-}Opx}$ = 892 °C), and intermediate temperatures near the ophiolite's metamorphic sole (T_{BKN} = 834 °C, $T_{Ca\text{-}in\text{-}Opx}$ = 961 °C). $T_{Ca\text{-}in\text{-}Ol}$ decrease from a high of 855 °C near the crust to a low of 633 °C in the middle of the section. Aside from a sample with a slightly higher temperature near the crust, $T_{Ol\text{-}Sp}$ shows no significant variation with depth, as is true for temperatures determined using the Al-in-opx thermometer of Witt-Eickschen and Seck (1991) (Table 1). However, the OM94 pyroxene compositions fall outside the calibration range of the empirical Al-in-opx thermometer.

Temperatures determined using the REE-in-two-pyroxene thermometer are plotted versus T_{BKN} and $T_{Ca\text{-}in\text{-}Opx}$ in Figs. 4a and 4b. In addition to samples from Oman and other ophiolites, abyssal peridotites and subcontinental peridotites from thermally stable environments are shown (plots for other thermometers are presented in Supplementary Fig. S1). The two OM94 samples nearest to the paleo-Moho have T_{BKN} and $T_{Ca\text{-}in\text{-}Opx}$ similar to those in abyssal peridotites and slightly higher T_{REE} than the abyssal peridotites. They have major element temperatures overlapping those for other samples from Oman but higher T_{REE}. Samples from the OM94 traverse deeper in the Wadi Tayin section record lower temperatures than abyssal peridotites, overlapping those of other ophiolites. The similar distribution of data in Figs. 4a and 4b demonstrates that the temperature systematics we observe are not an artifact of a particular thermometer (e.g., also see Supplementary Fig. S1c). Fig. 4c compares $T_{Ol\text{-}Sp}$ and $T_{Ca\text{-}in\text{-}Ol}$ for peridotites from Oman, other ophiolites, and abyssal peridotites. Oman samples have lower $T_{Ol\text{-}Sp}$ than many abyssal peridotites and lower $T_{Ca\text{-}in\text{-}Ol}$ than most abyssal peridotites, which is true of all ophiolites.

To interpret the physical meaning of the temperatures recorded by major and REE-based thermometers, we must consider the concept of closure temperature, and evaluate whether the temperatures we observe qualify as closure temperatures. Closure temperature is defined as the lower temperature limit at which diffusive exchange of an element (or component) between a mineral and its surroundings effectively ceases during cooling (Dodson, 1973). For a mineral surrounded by an effectively infinite reservoir, Dodson's equation for closure temperature, T_c, is given by

$$\frac{E}{RT_c} = \ln\left(\frac{ART_c^2 D_0}{Ea^2\dot{s}}\right), \tag{1}$$

where E and D_0 are the activation energy and the pre-exponential factor for diffusion of the element of interest, respectively; A is a geometric constant (here we assume a sphere); a is an effective grain size; $\dot{s}$ is the cooling rate at T_c; and R is the gas constant. In this formulation, T_c is the mean or average closure temperature across the mineral grain. We will use the mean closure temperature or closure temperature, for short, in our discussion below.

In a majority of published studies, temperatures derived from major or trace element-based thermometers for a sample are calculated using average concentrations based on chemical analysis of several mineral grains in a thin section. It is reasonable to interpret major element exchange thermometer temperatures as the mean closure temperatures or proxies for closure temperatures if (1) analytical quality is good and representative, and (2) the sample of interest had a simple thermal history, i.e., not disturbed by melt infiltration, metasomatism, or another geologic processes. T_{REE} are more difficult to interpret, as the REE-in-two-pyroxene thermometer depends on major and trace element exchange between two pyroxenes, and gives a single temperature for all REEs + Y. Numerical simulations of REE diffusive exchange between pyroxenes in cooling opx–cpx aggregates (Yao and Liang, 2015), and comparisons among natural samples from a variety of tectonic environments (including subcontinental mantle, mid-ocean ridge spreading centers, subduction zones, incipient rifts, and ophiolites, Dygert and Liang, 2015; Liang et al., 2013; Sun and Liang, 2015; Wang et al., 2015) indicate T_{REE} reflect average closure temperatures for diffusive exchange of REEs+Y between opx and cpx. This

Table 1
Temperatures and cooling rates.

Sample	Depth (m)	T_{REE}	1σ	$T_{Ca\text{-}in\text{-}OPX}$	T_{BKN}	$T_{Ca\text{-}in\text{-}Ol}$	$T_{Ol\text{-}Sp}$ [a]	T_{W77} [b]	T_{P37} [c]	$T_{Al\text{-}in\text{-}OPX}$ [d]	Weighted average opx radius (mm) [e]	Weighted average cpx radius (mm) [e]	dT/dt (°C/y) from T_{REE} and T_{BKN}	Olivine radius (mm) [f]	dT/dt (°C/y) from $T_{Ca\text{-}in\text{-}Ol}$
OM94-61	9565	1060	22	961	834	704	778	904	887	983	0.5	0.088	5.00E−03	0.15	2.37E−03
OM94-67	7860	1063	12	921	853	658	767	906	924	1062	0.8	0.29	2.73E−03	0.2	3.50E−04
OM94-74	6430	1080	65	909	766	695	784	850	860	952	0.43	0.125	6.92E−04	0.15	1.85E−03
OM94-79	4895	1104	36	892	769	633	767	851	835	1003	0.44	0.11	7.75E−04	0.1	6.27E−04
OM94-98	2880	1238	41	906	719	780	783	825	830	1010	0.6	0.058	– [g]	0.5	– [g]
OM94-101	2150	1232	6	982	816	706	780	881	861	948	0.43	0.070	6.92E−03	0.15	2.50E−03
OM94-106	970	1325	5	1074	973	791	811	990	1005	1016	0.5	0.50	2.50E−01	0.425	2.83E−03
OM94-114	520	1333	18	1127	1058	855	766	1055	1072	1026	1.15	0.16	2.84E−01	0.2	5.46E−02

[a] Calculated with the thermometer of Fabriès (1979) using olivine and spinel data from Hanghøj et al. (2010).
[b] Wells (1977).
[c] Eq. (37), Putirka (2008).
[d] Witt-Eickschen and Seck (1991). Note the pyroxene compositions are outside the calibration range for this thermometer.
[e] Grain size is estimated assuming the shortest bisector establishes the effective grain size. Grain size is weighted by the number of laser spots in a grain of a particular size.
[f] Single olivine grains or two grains of approximately the same size were analyzed.
[g] Cooling rate cannot be obtained for this sample, see main text.

is further supported by the small T_{REE} uncertainties for the OM94 samples, which depend on the linearity of the T_{REE} inversions (i.e., the consistency among T_{REE} given by individual REEs, Supplementary Fig. S11). Collectively, the new major and trace element data reported here (Fig. 3, Supplementary Tables S1 and S2), systematic variations of T_{REE}, $T_{Ca\text{-}in\text{-}Opx}$, T_{BKN}, and $T_{Ca\text{-}in\text{-}Ol}$ with depth (Fig. 2), and linearity of the temperature inversions suggest the T_{REE} temperatures recorded by the Wadi Tayin peridotites can also be considered closure temperatures (see discussion below for one or two exceptions and further analysis).

Closure temperatures from two thermometers can be used to estimate an average cooling rate for a sample by comparison of the temperatures. This method requires that (1) the relative reequilibration rates for the thermometers can be reasonably assumed, (2) the sample of interest was in chemical equilibrium at an initial high temperature and cooled to its closure temperature at a constant rate in a closed system, (3) the rate of grain growth is insignificant compared to the rate of cooling, and (4) grain size is known. Using approximate solutions to diffusion equations for bimineralic systems, Liang (2014) showed that for two minerals, diffusive reequilibration rates follow the "minor's rule", which states the mineral with the lesser amount of a trace element in the system controls the reequilibration timescale. This idea was further explored in numerical simulations of REE redistribution in two pyroxene systems by Yao and Liang (2015), and by Liang (2015), who developed a generalized closure temperature equation for bimineralic systems. These studies found that, except in peridotites with very little cpx ($\phi_{cpx}/\phi_{opx} < 0.05$, where ϕ is the volume fraction of the mineral), REE diffusion in opx determines reequilibration timescales for the REE-in-two-pyroxene thermometer. This is an intuitive result; because opx/cpx partition coefficients are generally <0.05 and decrease further with decreasing temperature (e.g., Sun and Liang, 2014), unless cpx abundance is very low, most REEs in peridotites reside in cpx. Thus, in cases where $\phi_{cpx}/\phi_{opx} > 0.05$, cpx can be treated as a semi-infinite reservoir for REEs and most temperature-sensitive reequilibration will take place in REE-poor opx. Calculated using bulk major element analyses from Hanghøj et al. (2010), normative cpx/opx for most OM94 samples are >0.08 (Supplementary Table S3). (These normative estimates may or may not be representative of the thin sections we analyzed, as the cpx/opx content of the subsamples used to make the thin sections may differ from the subsamples analyzed for bulk composition.) Because diffusion of REEs in opx is not sensitive to REE ionic radius (Cherniak and Liang, 2007), individual REEs should all record the same T_{REE} for a given sample with $\phi_{cpx}/\phi_{opx} > 0.05$. This is suggested by the linearity of the eight OM94 samples in the T_{REE} inversion diagrams (Supplementary Fig. S11).

An effective Arrhenius relation for inter or chemical diffusion of major elements involved in the two pyroxene thermometer of Brey and Köhler (1990) is difficult to interpret, as this thermometer relies on exchange of the enstatite component between coexisting cpx and opx, and growth of cpx along the pyroxene solvus during cooling. Cpx growth during cooling is only volumetrically significant relative to cpx present at magmatic temperatures for Ca-poor samples. According to mineral norms for OM94 peridotites (Supplementary Table S3), cpx grown at subsolidus temperatures is minor relative to cpx present at magmatic temperatures in 6 of the 8 samples investigated here. For the samples that experienced insignificant cpx growth during cooling, T_{BKN} closure temperatures may be reasonably approximated by Arrhenius relations for Ca–Mg–Fe exchange between diopside and enstatite. As diffusion data needed to model this exchange are not currently available, Dygert and Liang (2015) compared T_{BKN} for ophiolitic peridotites to closure temperatures calculated using Fe–Mg diffusion coefficients from 7 sources and Dodson's closure temperature equation, ultimately selecting an Arrhenius relation for Fe–Mg interdiffusion in

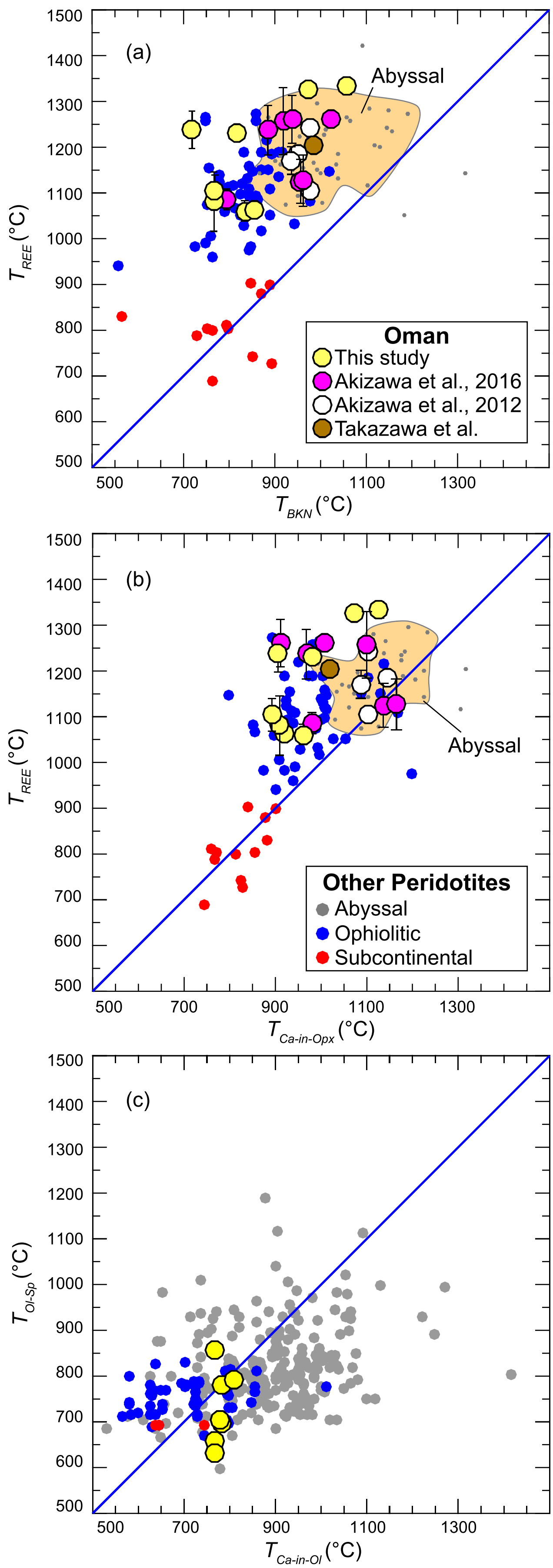

Fig. 4. Comparisons of temperatures derived from several geothermometers, additional comparisons are shown in Supplementary Fig. S1. Gray circles (highlighted by peach fields in (a) and (b)) are abyssal peridotites. Samples from Oman are large circles, other ophiolites are shown as blue circles, red circles are subcontinental peridotites. (a) T_{REE} plotted against T_{BKN}. Note that many samples from Oman have T_{REE} and T_{BKN} similar to abyssal peridotites. This suggests abyssal peridotites and Oman peridotites cooled at similar rates from initially high temperatures. In contrast, samples from many other ophiolites have T_{REE} similar to abyssal peridotites, but lower T_{BKN}. (b) T_{REE} plotted against $T_{Ca\text{-}in\text{-}Opx}$. As in (a), abyssal peridotites and some samples from Oman have similar temperatures, while many ophiolites have lower $T_{Ca\text{-}in\text{-}Opx}$ than the abyssal peridotites, demonstrating that the temperature systematics hold up for different thermometers. (c) A comparison of $T_{Ol\text{-}Sp}$ and $T_{Ca\text{-}in\text{-}Ol}$ temperatures. Because their parameterizations are based on fast-diffusing mineral components, these thermometers are more sensitive to the low temperature cooling history of a sample than the T_{REE}, $T_{Ca\text{-}in\text{-}Opx}$, and T_{BKN} thermometers. The figure shows that samples from Oman and other ophiolites have lower $T_{Ol\text{-}Sp}$ than many abyssal peridotites and lower $T_{Ca\text{-}in\text{-}Ol}$ than most abyssal peridotites, suggesting that in general, ophiolites cool more slowly than abyssal peridotites at low temperatures ($\lesssim$900 °C). Additional Oman data: Akizawa et al. (2016) are harzburgites from Wadi Fizh, Wadi Thuqbah, Wadi Rajmi, and Wadi Sarami in central and northern Oman. They were mostly collected at what are interpreted as paleo-spreading center segment ends. Three exceptions are from the central portion of the Thuqbah massif, among them, T_{REE} is highest in a sample closest to the paleo-Moho. Akizawa et al. (2012) are harzburgites from Wadi Fizh in the northern Samail ophiolite, ∼5 km W of the Moho (distance in map view); Takazawa et al. (2003) is from deformed Wadi Fizh lherzolites near the basal thrust. Data sources for other ophiolites and subcontinental peridotites are the following: Aldanmaz (2012), Barth et al. (2003), Batanova et al. (2011), Dygert and Liang (2015), Dygert et al. (2016), Jean et al. (2010), Khedr et al. (2014), Marchesi et al. (2011), Müntener et al. (2010), Riches and Rogers (2011), Takazawa et al. (2003). Data sources for abyssal peridotite T_{REE} are the following: Brunelli and Seyler (2010), D'Errico et al. (2016), Hellebrand et al. (2005), Seyler et al. (2011), Warren et al. (2009). Abyssal peridotite $T_{Ol\text{-}Sp}$ and $T_{Ca\text{-}in\text{-}Ol}$ are augmented with data for plagioclase-free samples from the compilation of Warren (2016). (For interpretation of the references to color in this figure legend, the reader is referred to the web version of this article.)

cpx (Dimanov and Wiedenbeck, 2006). This choice best matches temperatures in T_{REE} and T_{BKN} space recorded by slow cooling peridotites. According to Eq. (1), they should converge to a line left of and sub-parallel to the 1:1 line in Fig. 5 (also see Fig. 8 in Dygert and Liang, 2015). Choosing an Arrhenius relation allows us to calculate cooling rates which should be accurate relative to each other for OM94 samples that are not very cpx poor.

Fig. 5 presents closure curves constructed using a modified form of Dodson's equation (Ganguly and Tirone, 1999), which models the dependence of closure temperature (T_c) on grain size, initial temperature, and cooling rate, assuming the closure of T_{REE} are rate-limited by diffusion of REEs in opx (Cherniak and Liang, 2007) and the closure of T_{BKN} are approximated by diffusion of Fe–Mg in cpx (Dimanov and Wiedenbeck, 2006). We emphasize that (1) this method assumes one-stage cooling at constant rates and grain size, (2) gives an average cooling rate over the temperature interval recorded by the thermometers. Closure curves are presented for a range of initial temperatures (as indicated right of the 1:1 line). Numbers above the hottest cooling curve are cooling rates in °C/y. As demonstrated by the closure curves, the position of a sample in temperature space generally indicates its relative cooling rate, with samples farther from the 1:1 line experiencing slower cooling. These closure curves were calculated for an effective and constant grain radius of 0.5 mm but can be scaled to other grain sizes as T_c varies with radius squared (Eq. (1)). Because pyroxene grain size varies by orders of magnitude among natural samples, scaling to measured grain sizes is critical when using this method to estimate cooling rates.

Assuming one-stage cooling, the path of a sample in temperature space is as follows: Starting on the 1:1 line, it moves left along a cooling curve corresponding to its initial temperature. If it cools sufficiently slowly, the sample will then move diagonally downward along the curve given by Eq. (1). Samples that fall to the left of the cooling curves may record closure temperatures that are not meaningful due to geochemical disturbance (e.g., melt-rock interaction), data quality issues, complex cooling histories that

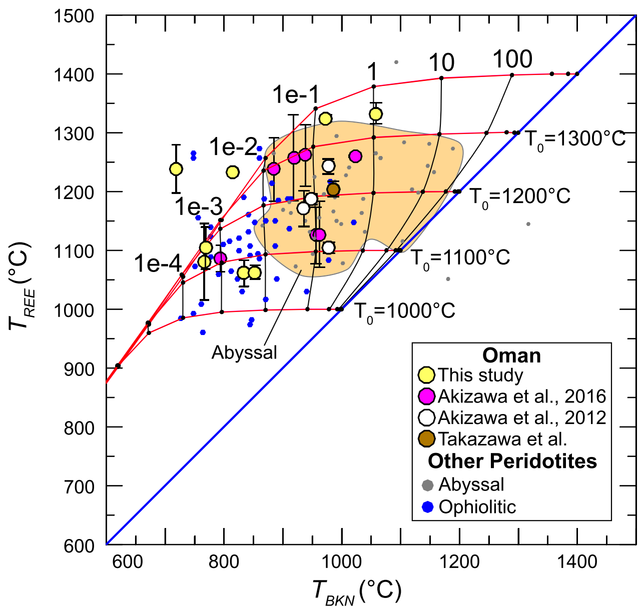

Fig. 5. Closure temperature cooling curves calculated using the method of Dygert and Liang (2015) overlaid on measured closure temperatures for the REE and BKN thermometers. Calculations were made assuming the cooling rate was constant throughout the cooling interval recorded by these two thermometers. Initial temperatures (T_0) for each cooling curve are indicated right of the blue 1:1 line. Cooling rates calculated for a 0.5 mm radius opx grain (°C/y) are indicated above the highest cooling curve; divide by 100 to rescale cooling rates for 5 mm radius grains. For reference, the OM94 opx we analyzed have (on average) radii of 0.425–1.15 mm (Table 1, Supplementary Figs. S7–S10); the abyssal peridotites apparently have larger radii (up to 7.5–10 mm according to Hellebrand et al., 2005 and Brunelli and Seyler, 2010). Black lines originating from the $T_0 = 1400\,°C$ cooling curve indicate cooling rates for lower T_0. At slow cooling rates, the curves converge to Eq. (1) (Dodson, 1973), the line left of and sub-parallel to the 1:1 line. Cooling curves were calculated with the closure temperature model of Ganguly and Tirone (1999) using diffusion data for REE in opx for T_{REE} (Cherniak and Liang, 2007) and diffusion data for Fe–Mg interdiffusion in cpx for T_{BKN} (Dimanov and Wiedenbeck, 2006) (see explanation in the main text). Cpx in sample OM94-98, which plots left of the cooling curves, may have exsolved from opx at low temperature (cf. Supplementary Fig. S8). A meaningful cooling rate for this sample cannot be determined. (For interpretation of the references to color in this figure legend, the reader is referred to the web version of this article.)

are difficult to interpret using closure temperatures alone, or have been cpx-free at magmatic temperatures. It is important to reiterate the need for accurate diffusion data in modeling the closure of relevant major and trace elements in the two-pyroxene systems. Future study should also consider effects of major element composition and pressure on cation diffusion and closure temperatures in pyroxenes.

Five of the eight OM94 samples plot along a single cooling curve corresponding to an apparent initial temperature of ∼1330 °C. We interpret the three outliers as follows: The sample that falls far to the left of the cooling curve (OM94-98) has small cpx (80–150 μm in diameter) hosted by large opx grains (Supplementary Fig. S7) and low bulk Ca, suggesting all of its cpx exsolved from opx at subsolidus temperatures. In a scenario where cpx grows from opx at low temperature, REEs are likely to be depleted in a metamorphic halo in the host opx immediately surrounding the growing cpx grain. This would starve the growing cpx of REEs. Because opx/cpx REE partition coefficients decrease with decreasing temperature (Eggins et al., 1998; Sun and Liang, 2014; Witt-Eickschen and O'Neill, 2005), analysis of cpx with artificially low REE concentrations in cpx, together with "correct" REE concentrations in opx away from the depletion halo, would lead to artificially high T_{REE}. Such a sample would also have a low T_{BKN}. Thus, we infer that OM94-98 does not provide closure temperatures relevant to the high-temperature cooling history of the ophiolite. The other two samples that plot away from the cooling curve defined by five samples, to the right of the cooling curve (OM94-61, OM94-67), are at the base of the mantle section of the ophiolite, near the metamorphic sole. Thus, these two samples may record a thermal disturbance related to obduction. (We caution that one of these samples, OM94-61, has low bulk Ca and may have been cpx-free at magmatic temperatures.)

Apparent cooling rates obtained from the closure curves (corrected for measured grain sizes) are plotted as a function of distance from the paleo-Moho in Fig. 6 (red and blue squares), and presented in Table 1. The cooling rates mimic the closure temperatures; they are high near the paleo-Moho (∼0.3 °C/y), gradually decreasing to a minimum in the middle of the section (∼10^{-3} °C/y) before an apparent increase at the base (∼5×10^{-3} °C/y). Shown for comparison are cooling rates obtained using Ca-in-olivine thermometry (Köhler and Brey, 1990) and Dodson's (1973) equation (white and green circles) using a diffusion coefficient for Ca in olivine from Coogan et al. (2005b) (parallel to *c*-axis). Rates for samples from the crustal section (unfilled circles, VanTongeren et al., 2008) agree with rates for the mantle section (green circles, this study), and the fast cooling rates obtained using T_{REE} and T_{BKN} for peridotites closest to the Moho. This consistency is striking, especially as the cooling rates were obtained using different minerals, thermometers, and methods.

Previous studies applying olivine-spinel geospeedometers to ophiolitic peridotites have obtained cooling rates somewhat consistent with our results. Investigating dunites from Wadi Bani Kharus in the Nakhl massif of the Samail ophiolite in Oman, Coogan et al. (2007b) found rates of ∼10^{-2} °C/y near the Moho, ∼10^{-3} °C/y in the interior of the mantle section, and ∼10^{-2} °C/y at the basal thrust. Ozawa (1984) found cooling rates of ∼10^{-4}–10^{-2} °C/y for peridotites from several Japanese ophiolites (Horoman, Iwanaidake, and Miyamori). Rapid Fe–Mg diffusion makes olivine-spinel thermometers sensitive to low temperature cooling processes and spinel grain size, which may explain some of the inconsistency with our observations; choice of diffusion data also significantly affects calculated cooling rates.

4. Interpretations

Our next task is to understand what physical processes could have brought about the spatial variations in closure temperatures and cooling rates with depth in the mantle section. The cooling history of the oceanic upper mantle is intimately related to the cooling history of the overlying crust. A body of literature has explored the thermal history of the oceanic crust in an effort to evaluate mechanisms of crustal accretion (e.g., Coogan et al., 2002, 2007b; Faak et al., 2015; Faak and Gillis, 2016; Garrido et al., 2001; VanTongeren et al., 2008). There are two end-member crustal accretion models; in the Gabbro Glacier model, lower oceanic crust accretes from crystallization in a single magma chamber beneath the axis of a spreading center (Henstock et al., 1993; Phipps Morgan and Chen, 1993; Quick and Denlinger, 1993; Sinton and Detrick, 1992; Sleep, 1975). Newly formed crust advects downward from the magma chamber floor and away from the ridge axis as seafloor spreading progresses. In contrast, in the Sheeted Sills model, oceanic crust accretes from crystallization of small sills at many depths within the lower crust, and the sills were emplaced at depths they are observed today (Kelemen et al., 1997a, 1997b; Korenaga and Kelemen, 1998; VanTongeren et al., 2008, 2015). Hybrid models that combine features of these two end-members have also been proposed (e.g., Boudier et al., 1996). In fact, even the schematic sheeted sill illustrations of Kelemen et al. (1997a, 1997b) and Korenaga and Kelemen (1998) include a small gabbro glacier forming the uppermost part of the plutonic oceanic crust.

The end-member crustal accretion models have different requirements for crustal cooling. The Sheeted Sills model requires

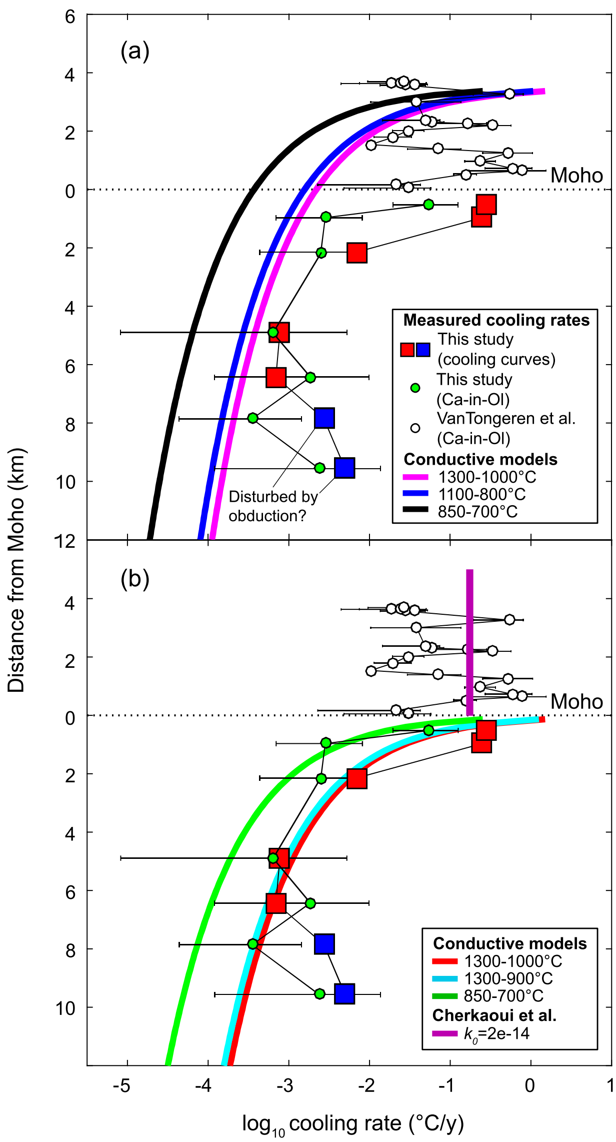

Fig. 6. Cooling rates of OM94 peridotites based on REE and BKN thermometry (red and blue squares, Table 1 and Fig. 5) and Ca-in-Ol thermometry (green circles) based on olivine-cpx Ca/Mg exchange. Also shown are rates for crustal gabbros (white circles; VanTongeren et al., 2008). Measured cooling rates are compared to cooling rates modeled using Eq. (2), and from Cherkaoui et al. (2003). Conductive cooling models assume a thermal diffusivity of 1×10^{-6} and an initial temperature of 1350 °C. Blue squares are samples that may have cooling histories affected by the obduction process. (a) Comparison with models that assume conductive cooling of the lower crust and mantle. We assume hydrothermal circulation is pervasive in the upper oceanic crust and fix the temperature 2.5 km beneath the seafloor at 200 °C. The results are almost identical in simulations where temperature is fixed at 0 °C at the same depth. These models underestimate cooling rates of the lower crust and mantle. (b) Comparison with models that assume the entire crust cools by hydrothermal circulation. In the model of Cherkaoui et al. (2003), the crust has a permeability of 1×10^{-14} m^2. The conductive models assume cooling of the mantle into a cold overlying crust with a constant temperature (200 °C). Again, the results are almost identical in simulations where temperature at the crust–mantle interface is fixed at 0 °C or 350 °C. (For interpretation of the references to color in this figure legend, the reader is referred to the web version of this article.)

deep and efficient hydrothermal circulation beneath the ridge axis to accommodate latent heat produced by crystallization of the sills (e.g., Maclennan et al., 2004). The Gabbro Glacier model requires that immediately beneath the ridge axis, hydrothermal circulation is limited to the extrusive section of the crust, while the lower crust and underlying mantle cool mainly by conduction. (This might not preclude deep hydrothermal circulation within a few km of the mid-ocean ridge axis around a very tall and narrow Gabbro Glacier, Buck, 2000.) Making the simplifying assumptions that the lower crust and the uppermost mantle have the same initial temperature, and that heat conduction in the direction of seafloor spreading can be neglected, we can test whether the observed cooling rates are consistent with conductive cooling of the crust and mantle (and by extension, the Gabbro Glacier model) using a half-space solution to the one-dimensional heat conduction equation,

$$T = (T_1 - T_0) \times erf\left(\frac{z}{2\sqrt{\kappa t}}\right) + T_0, \tag{2}$$

where T_1 is the initial temperature of the rock and T_0 is the temperature at the rock–seawater interface; z is the depth beneath the seafloor; t is time; and κ is thermal diffusivity (Eq. 4-125, Turcotte and Schubert, 2002). Taking the derivative of Eq. (2) with respect to time gives the instantaneous cooling rate, which varies nonlinearly in time at a given z. More useful is an average cooling rate calculated over the observed T_{REE}, T_{BKN}, and $T_{Ca\text{-}in\text{-}Ol}$ closure temperature intervals of our samples.

The results of several models for conductive cooling of the lower crust and mantle are presented in Fig. 6a. Average cooling rates calculated over high temperature cooling intervals (e.g., the magenta line, 1300–1000 °C) are faster than cooling rates calculated over lower temperature intervals (e.g., the black line, 850–700 °C). These models underestimate cooling rates recorded by crust and mantle rocks throughout the section, more importantly, they fail to match the spatial variation of cooling rate with depth. We conclude that purely conductive cooling of the lower crust and mantle is inconsistent with the closure temperatures and cooling rates preserved at Wadi Tayin, suggesting the lower crust in that section was not emplaced in a gabbro glacier.

A crustal cooling model from Cherkaoui et al. (2003) is shown in Fig. 6b (purple vertical line). Cherkaoui et al. (2003) incorporated both heat conduction and hydrothermal circulation in their models, which provide a better match than purely conductive cooling models to the crustal closure temperatures and corresponding cooling rates of VanTongeren et al. (2008) in the Wadi Tayin massif. Intrigued by these results, we calculated cooling rate profiles for the mantle assuming conductive cooling of the mantle section below the Moho, overlain by a cold lower crust with constant temperature. (We used 200 °C, based on Cherkaoui et al., 2003; crustal temperatures between 0 and 350 °C would provide similar results.) The correspondence between the models and the curvature and magnitude of the cooling rate profiles suggests that the Wadi Tayin mantle section cooled by conduction below a cold overlying crust, in agreement with the Sheeted Sills model and the data of VanTongeren et al. (2008). These findings are consistent with a recent investigation of lattice-preferred orientations in Wadi Tayin crustal gabbros (VanTongeren et al., 2015), which found no evidence for the plagioclase *a*-axis alignment that would be produced by advection of crust from an axial magma chamber (required by the Gabbro Glacier model). Instead, in the lower crust, girdles defined by plagioclase *a*-axes are perpendicular to the paleo-Moho, consistent with the Sheeted Sills model.

Samples nearest to the paleo-Moho (which have $T_{REE} > 1300$ °C) experienced very fast cooling that effectively froze REE abundances in coexisting pyroxenes at magmatic temperatures. Seawater infiltration caused by faulting would rapidly cool the mantle, but may also produce a cooling rate profile with near-constant, fast cooling rates, unlike the gradual, systematically decreasing cooling rates we observe (Fig. 6). Our observations are most consistent with efficient hydrothermal circulation that extended to (but not far beneath) the base of the crustal section. Serpentinization of the mantle at the paleo-Moho (and the associated volume increase) may have formed a barrier to deeper circulation of seawater, preventing hydrothermal cooling of the mantle, as previously proposed by Hanghøj et al. (2010). Thus, serpentinization of ophiolitic peridotites may largely take place off axis, perhaps during or after obduction.

Although the presently available data are admittedly limited, we interpret the pyroxene solvus temperatures, with the associated, apparent increase in cooling rates at the base of the section, as reflecting a late thermal disturbance related to obduction. The samples may have been heated from below by frictional sliding along the ophiolitic sole after earlier closure of the major and trace element thermometers. Because of the slow diffusion of REEs compared to major elements, this could increase T_{BKN} at $\sim$ constant T_{REE}, moving the samples from the Dodson (1973) closure temperature cooling curve rightward toward the 1:1 line (Fig. 5). Alternatively, the samples may have been quenched from below during obduction, requiring initiation of basal thrusting while the mantle lithosphere was still young and hot (e.g., Hacker et al., 1996).

Finally we turn to the $T_{Ol\text{–}Sp}$ and $T_{Ca\text{-}in\text{–}Ol}$ systematics (Fig. 4c). The Ol–Sp and Ca-in-Ol thermometers are based on exchange of relatively fast-diffusing mineral components and are thus typically sensitive to cooling at temperatures $<1000\,^\circ$C (at mantle-relevant cooling rates). In general, $T_{Ol\text{–}Sp}$ and $T_{Ca\text{-}in\text{–}Ol}$ are lower for ophiolites than abyssal peridotites as noted previously by Hanghøj et al. (2010), suggesting that ophiolites cool more slowly than abyssal peridotites at temperatures $<1000\,^\circ$C. This presents an interesting contrast to cooling of ophiolitic peridotites and abyssal peridotites at high temperatures, which appears to occur at similar rates. Perhaps hydrothermal cooling at the base of ophiolite crusts slows or stops during obduction, whereas rapid cooling of peridotites in abyssal environments continues as they migrate to the seafloor by tectonic exhumation.

5. Summary and conclusions

Abyssal peridotites and samples from the mantle section of the Wadi Tayin massif of the Samail ophiolite in Oman appear to have experienced similar high temperature cooling histories (Dygert and Liang, 2015). Because abyssal peridotites are dredged from amagmatic environments while the Oman ophiolite has a thick crust, the cooling rate of the mantle beneath mid-ocean ridges in the temperature interval from $\sim$1300 to $\sim$1000 °C appears to be independent of spreading rate or the presence or absence of crust. To understand what physical mechanisms cool the mantle beneath mid-ocean ridges, we applied the REE-in-two-pyroxene thermometer of Liang et al. (2013) and major element thermometers of Brey and Köhler (1990), Köhler and Brey (1990), and Fabriès (1979) to peridotites from a transect through the mantle section of the Wadi Tayin massif in the southern Samail ophiolite in Oman. Corrected for structural depth, the section represents 10 km of mantle stratigraphy, making it suitable for investigating physical controls on cooling. Samples exhibit a statistically significant gradient in major element and REE-in-two-pyroxene closure temperatures, with $T_{REE} > 1300\,^\circ$C near the paleo-Moho and $<1100\,^\circ$C at the base of the section. Based on cooling curves constructed using Arrhenius relations for REE and Fe–Mg diffusion in pyroxene, we estimated cooling rates which vary systematically throughout the section. The uppermost mantle was cooled from high temperature at a rate ($\sim$0.3 °C/y) consistent with previous estimates for the crust (VanTongeren et al., 2008). Cooling was slowest $\sim$6 km beneath the paleo-Moho ($\sim 10^{-3}$ °C/y) and may have been slightly faster near the ophiolitic sole ($\sim 5 \times 10^{-3}$ °C/y). Cooling rates calculated for the Ca-in-olivine thermometer are slower, and also decrease moving deeper into the section.

We used half-space cooling models to better understand our observations, which demonstrate that conductive cooling alone underestimates cooling rates of rocks in the crust and mantle. The spatial variation in cooling rates can be explained by conductive heat loss from the mantle into a cold overlying crust, suggesting hydrothermal circulation extended to (but not far beneath) the Moho at the ridge axis. These observations are most consistent with the Sheeted Sills model for accretion of oceanic crust. A lack of hydrothermal circulation beneath the Moho near the ridge axis suggests serpentinization of the mantle in ophiolites must largely take place off axis, perhaps during or after obduction. Fast cooling at the base of the mantle section can be attributed to frictional heating during obduction, or quenching associated with emplacement of the ophiolite along the basal thrust while the mantle was still hot. This study suggests that efficient hydrothermal cooling of the crust beneath mid-ocean ridges cools the uppermost mantle through the temperature interval from $\sim$1300 to 1000 °C as quickly as tectonic exhumation in amagmatic environments. Thermometers based on fast diffusing cations seem to record lower closure temperatures and slower cooling rates for ophiolite samples compared to exhumed peridotites, perhaps because hydrothermal cooling slowed at the base of ophiolite crust during obduction, whereas rapid cooling of peridotites in abyssal environments due to tectonic exhumation continued to the seafloor. Overall, our new data demonstrate that the REE-in-two pyroxene thermometer is a powerful tool for unraveling the high-temperature cooling history of ultramafic rocks, placing new constraints on important tectonic and geophysical processes. We hope this work motivates new efforts to model hydrothermal cooling beneath mid-ocean ridges, more detailed investigations into the cooling histories of ophiolites and abyssal peridotites, and additional studies of cation diffusion in pyroxene.

Acknowledgements

We thank Nathaniel Miller for assistance with LA-ICP-MS analyses. This paper benefited from thoughtful reviews by Kathi Faak and an anonymous reviewer, and editorial handling by Mike Bickle. This work was supported by a Jackson School of Geosciences postdoctoral fellowship to N.D., NSF grant EAR-1632815 to Y.L., and NSF grants EAR-1516300, EAR-1049905, Alfred P. Sloan Foundation Grant 2014-3-01, and International Continental Drilling Program grant "Oman Drilling Project" to P.B.K.

Appendix A. Supplementary material

Supplementary material related to this article can be found online at http://dx.doi.org/10.1016/j.epsl.2017.02.038.

References

Akizawa, N., Arai, S., Tamura, A., 2012. Behavior of MORB magmas at uppermost mantle beneath a fast-spreading axis: an example from Wadi Fizh of the northern Oman ophiolite. Contrib. Mineral. Petrol. 164 (4), 601–625. http://dx.doi.org/10.1007/s00410-012-0762-4.

Akizawa, N., Ozawa, K., Tamura, A., Michibayashi, K., Arai, S., 2016. Three dimensional evolution of melting, heat and melt transfer in ascending mantle beneath a fast-spreading ridge segment constrained by trace elements in clinopyroxene from concordant dunites and host harzburgites of the Oman ophiolite. J. Petrol. 57, 777–814. http://dx.doi.org/10.1093/petrology/egw020.

Aldanmaz, E., 2012. Trace element geochemistry of primary mantle minerals in spinel-peridotites from polygenetic MOR-SSZ suites of SW Turkey: constraints from an LA-ICP-MS study and implications for mantle metasomatism. Geol. J. 46, 59–76. http://dx.doi.org/10.1002/gj.1336.

Barth, M.G., Mason, P.R.D., Davies, G.R., Dijkstra, A.H., Drury, M.R., 2003. Geochemistry of the Othris Ophiolite, Greece: evidence for refertilization? J. Petrol. 44, 1759–1785. http://dx.doi.org/10.1093/petrology/egg058.

Batanova, V.G., Belousov, I.A., Savelieva, G.N., Sobolev, A.V., 2011. Consequences of channelized and diffuse melt transport in supra-subduction zone mantle: evidence from the Voykar Ophiolite (Polar Urals). J. Petrol. 52, 2483–2521. http://dx.doi.org/10.1093/petrology/egr053.

Boudier, F., Nicolas, A., Idelfonse, B., 1996. Magma chambers in the Oman ophiolite: fed from the top and the bottom. Earth Planet. Sci. Lett. 144, 239–250. http://dx.doi.org/10.1016/0012-821X(96)00167-7.

Boyd, F.R., 1973. A pyroxene geotherm. Geochim. Cosmochim. Acta 37 (12), 2533–2546. http://dx.doi.org/10.1016/0016-7037(73)90263-9.

Braun, M.G., 2004. Petrologic and Microstructural Constraints on Focused Melt Transport in Dunites and the Rheology of the Shallow Mantle. PhD Thesis, MIT-WHOI Joint Program.

Brey, G.P., Köhler, T., 1990. Geothermobarometry in four-phase lherzolites II. New thermobarometers, and practical assessment of existing thermobarometers. J. Petrol. 31 (6), 1353–1378. http://dx.doi.org/10.1093/petrology/31.6.1353.

Brunelli, D., Seyler, M., 2010. Asthenospheric percolation of alkaline melts beneath the St. Paul region (Central Atlantic Ocean). Earth Planet. Sci. Lett. 289, 393–405.

Buck, W.R., 2000. Can downward flow of dense cumulate slurry through mush upper gabbros produce lower gabbros at a fast-spreading center? In: Dilek, Y., et al. (Eds.), Ophiolites and Oceanic Crust: New Insights from Field Studies and the Ocean Drilling Program. In: Spec. Pap., Geol. Soc. Am., vol. 349. GSA, Boulder, Colorado, pp. 121–127.

Chakraborty, S., 2010. Diffusion coefficients in olivine, wadsleyite and ringwoodite. Rev. Mineral. Geochem. 72, 603–639. http://dx.doi.org/10.2138/rmg.2010.72.13.

Cherkaoui, A.S.M., Wilcock, W.S.D., Dunn, R.A., Toomey, D.R., 2003. A numerical model of hydrothermal cooling and crustal accretion at a fast spreading mid-ocean ridge. Geochem. Geophys. Geosyst. 4 (9), 8616. http://dx.doi.org/10.1029/2001GC000215.

Cherniak, D.J., Liang, Y., 2007. Rare earth element diffusion in natural enstatite. Geochim. Cosmochim. Acta 71, 1324–1340. http://dx.doi.org/10.1016/j.gca.2006.12.001.

Cherniak, D.J., Dimanov, A., 2010. Diffusion in pyroxene, mica and amphibole. Rev. Mineral. Geochem. 72, 641–690. http://dx.doi.org/10.2138/rmg.2010.72.14.

Coogan, L.A., Jenkin, G.R.T., Wilson, R.N., 2002. Constraining the cooling rate of the lower oceanic crust: a new approach applied to the Oman ophiolite. Earth Planet. Sci. Lett. 199, 127–146. http://dx.doi.org/10.1016/S0012-821X(02)00554-X.

Coogan, L.A., Kasemann, S.A., Chakraborty, S., 2005a. Rates of hydrothermal cooling of new oceanic upper crust derived from lithium-geospeedometry. Earth Planet. Sci. Lett. 240, 415–424. http://dx.doi.org/10.1016/j.epsl.2005.09.020.

Coogan, L.A., Hain, A., Stahl, S., Chakraborty, S., 2005b. Experimental determination of the diffusion coefficient for calcium in olivine between 900 °C and 1500 °C. Geochim. Cosmochim. Acta 69 (14), 3683–3694. http://dx.doi.org/10.1016/j.gca.2005.03.002.

Coogan, L.A., Manning, C.E., Wilson, R.N., E.I.M.F., 2007a. Oxygen isotope evidence for short-lived high-temperature fluid flow in the lower oceanic crust at fast-spreading ridges. Earth Planet. Sci. Lett. 260, 524–536. http://dx.doi.org/10.1016/j.epsl.2007.06.013.

Coogan, L.A., Jenkin, G.R.T., Wilson, R.N., 2007b. Contrasting cooling rates in the lower oceanic crust at fast- and slow-spreading ridges revealed by geospeedometry. J. Petrol. 48 (11), 2211–2231. http://dx.doi.org/10.1093/petrology/egm057.

D'Errico, M.E., Warren, J.M., Godard, M., 2016. Evidence for chemically heterogeneous Arctic mantle beneath the Gakkel Ridge. Geochim. Cosmochim. Acta 174, 291–312. http://dx.doi.org/10.1016/j.gca.2015.11.017.

Dick, H.J.B., Bullen, T., 1984. Chromian spinel as a petrogenetic indicator in abyssal and alpine-type peridotites and spatially associated lavas. Contrib. Mineral. Petrol. 86, 54–76. http://dx.doi.org/10.1007/BF00373711.

Dimanov, A., Wiedenbeck, M., 2006. (Fe, Mn)-Mg interdiffusion in natural diopside: effect of pO_2. Eur. J. Mineral. 18, 705–718. http://dx.doi.org/10.1127/0935-1221/2006/0018-0705.

Dodson, M.H., 1973. Closure temperature in cooling geochronological and petrological systems. Contrib. Mineral. Petrol. 40, 259–274. http://dx.doi.org/10.1007/BF00373790.

Dygert, N., Liang, Y., 2015. Temperatures and cooling rates recorded in REE in coexisting pyroxenes in ophiolitic and abyssal peridotites. Earth Planet. Sci. Lett. 420, 151–161. http://dx.doi.org/10.1016/j.epsl.2015.02.042.

Dygert, N., Liang, Y., Kelemen, P.B., 2016. Formation of plagioclase lherzolite and associated dunite–harzburgite–lherzolite sequences by multiple episodes of melt percolation and melt–rock reaction: an example from the Trinity ophiolite, California, USA. J. Petrol. 57, 815–838. http://dx.doi.org/10.1093/petrology/egw018.

Eggins, S.M., Rudnik, R.L., McDonough, W.F., 1998. The composition of peridotites and their minerals: a laser-ablation ICP-MS study. Earth Planet. Sci. Lett. 154, 53–71. http://dx.doi.org/10.1016/S0012-821X(97)00195-7.

Faak, K., Coogan, L.A., Chakraborty, S., 2015. Near conductive cooling rates in the upper-plutonic section of crust formed at the East Pacific Rise. Earth Planet. Sci. Lett. 423, 36–47. http://dx.doi.org/10.1016/j.epsl.2015.04.025.

Faak, K., Gillis, K.M., 2016. Slow cooling of the lowermost oceanic crust at the fast-spreading East Pacific Rise. Geology 44, 115–118. http://dx.doi.org/10.1130/G37353.1.

Fabriès, J., 1979. Spinel-olivine geothermometry in peridotites from ultramafic complexes. Contrib. Mineral. Petrol. 69, 329–336.

Ganguly, J., Tirone, M., 1999. Diffusion closure temperature and age of a mineral with arbitrary extent of diffusion: theoretical formulation and applications. Earth Planet. Sci. Lett. 170, 131–140. http://dx.doi.org/10.1016/S0012-821X(99)00089-8.

Garrido, C.J., Kelemen, P.B., Hirth, G., 2001. Variation of cooling rate with depth in lower crust formed at an oceanic spreading ridge: plagioclase crystal size distributions in gabbros from the Oman ophiolite. Geochem. Geophys. Geosyst. 2 (10). http://dx.doi.org/10.1029/2000GC000136.

Godard, M., Jousselin, D., Bodinier, J.-L., 2000. Relationships between geochemistry and structure beneath a paleo-spreading centre; a study of the mantle section in the Oman Ophiolite. Earth Planet. Sci. Lett. 180, 133–148. http://dx.doi.org/10.1016/S0012-821X(00)00149-7.

Hacker, B.R., Mosenfelder, J.L., Gnos, E., 1996. Rapid emplacement of the Oman ophiolite: thermal and geochronologic constraints. Tectonics 15 (6), 1230–1247. http://dx.doi.org/10.1029/96TC01973.

Hanghøj, K., Kelemen, P.B., Hassler, D., Godard, M., 2010. Composition and genesis of depleted mantle peridotites from the Wadi Tayin Massif, Oman ophiolite; major and trace element geochemistry, and Os isotopes and PGE systematics. J. Petrol. 51 (1–2), 201–227. http://dx.doi.org/10.1093/petrology/egp007.

Hellebrand, E., Snow, J.E., Mostefaoui, S., Hoppe, P., 2005. Trace element distribution between orthopyroxene and clinopyroxene in peridotites from the Gakkel Ridge: a SIMS and NanoSIMS study. Contrib. Mineral. Petrol. 150, 486–504.

Henstock, T.J., Woods, A.W., White, R.S., 1993. The accretion of oceanic crust by episodic sill intrusion. J. Geophys. Res. 98 (B3), 4143–4161. http://dx.doi.org/10.1029/92JB02661.

Jean, M.M., Shervais, J.W., Choi, S.-H., Mukasa, S.B., 2010. Melt extraction and melt refertilization in mantle peridotite of the Coast Range ophiolite: an LA-ICP-MS study. Contrib. Mineral. Petrol. 159, 113–136.

Kelemen, P.B., Shimizu, N., Salters, V.J.M., 1995. Extraction of mid-ocean-ridge basalt from the upwelling mantle by focused flow of melt in dunite channels. Nature 375, 747–753. http://dx.doi.org/10.1038/375747a0.

Kelemen, P.B., Hirth, G., Shimizu, N., Spiegelman, M., Dick, H.J.B., 1997a. A review of melt migration processes in the adiabatically upwelling mantle beneath oceanic spreading ridges. Philos. Trans. R. Soc. Lond. 355, 283–318. http://dx.doi.org/10.1089/rsta.1997.0010.

Kelemen, P.B., Koga, K., Shimizu, N., 1997b. Geochemistry of gabbro sills in the crust–mantle transition zone of the Oman ophiolite: implications for the origin of the oceanic lower crust. Earth Planet. Sci. Lett. 146, 475–488. http://dx.doi.org/10.1016/S0012-821X(96)00235-X.

Khedr, M.Z., Arai, S., Python, M., Tamura, A., 2014. Chemical variations of abyssal peridotites in the central Oman ophiolite: evidence of oceanic mantle heterogeneity. Gondwana Res. 25, 1242–1262.

Koga, K.T., Kelemen, P.B., Shimizu, N., 2001. Petrogenesis of the crust–mantle transition zone and the origin of lower crustal wehrlite in the Oman ophiolite. Geochem. Geophys. Geosyst. 2 (9). http://dx.doi.org/10.1029/2000GC000132.

Köhler, T.P., Brey, G.P., 1990. Calcium exchange between olivine and clinopyroxene calibrated as a geothermometer for natural peridotites from 2 to 60 kb with applications. Geochim. Cosmochim. Acta 54 (9), 2375–2388. http://dx.doi.org/10.1016/0016-7037(90)90226-B.

Korenaga, J., Kelemen, P.B., 1997. Origin of gabbro sills in the Moho transition zone of the Oman ophiolite: implications for magma transport in the oceanic lower crust. J. Geophys. Res. 102 (B12), 27729–27749. http://dx.doi.org/10.1029/97JB02604.

Korenaga, J., Kelemen, P.B., 1998. Melt migration through the oceanic lower crust: a constraint from melt percolation modeling with finite solid diffusion. Earth Planet. Sci. Lett. 156, 1–11. http://dx.doi.org/10.1016/S0012-821X(98)00004-1.

Lasaga, A.C., 1983. Geospeedometry: an extension of geothermometry. In: Saxena, S.K. (Ed.), Kinetics and Equilibrium in Mineral Reactions. In: Advances in Physical Geochemistry, vol. 3. Springer, New York, pp. 81–114.

Lee, C.T.A., Harbert, A., Leeman, W.P., 2007. Extension of lattice strain theory to mineral/mineral rare-earth element partitioning: an approach for assessing disequilibrium and developing internally consistent partition coefficients between olivine, orthopyroxene, clinopyroxene and basaltic melt. Geochim. Cosmochim. Acta 71, 481–496. http://dx.doi.org/10.1016/j.gca.2006.09.014.

Liang, Y., Sun, C., Yao, L., 2013. A REE-in-two-pyroxene thermometer for mafic and ultramafic rocks. Geochim. Cosmochim. Acta 102, 246–260. http://dx.doi.org/10.1016/j.gca.2012.10.035.

Liang, Y., 2014. Time scales of diffusive re-equilibration in bi-mineralic systems with and without a fluid or melt phase. Geochim. Cosmochim. Acta 132, 274–287. http://dx.doi.org/10.1016/j.gca.2014.02.008.

Liang, Y., 2015. A simple model for closure temperature of a trace element in cooling bi-mineralic systems. Geochim. Cosmochim. Acta 165, 35–43.

Lindsley, D.H., 1983. Pyroxene thermometry. Am. Mineral. 68, 477–493.

Lindsley, D.H., Anderson, D.J., 1983. A two-pyroxene thermometer. J. Geophys. Res. 88, A887–A906.

Maclennan, J., Hulme, T., Sing, S.C., 2004. Thermal models of oceanic crustal accretion: linking geophysical, geological and petrological observations. Geochem. Geophys. Geosyst. 5. http://dx.doi.org/10.1029/2003GC000605.

MacLeod, C.J., Lissenberg, C.J., Bibby, L.E., 2013. "Moist MORB" axial magmatism in the Oman ophiolite: the evidence against a mid-ocean ridge origin. Geology 41, 459–462. http://dx.doi.org/10.1130/G33904.i.

Marchesi, C., Jolly, W.T., Lewis, J.F., Garrido, C.J., Proenza, J.A., Lidiak, E.G., 2011. Petrogenesis of fertile mantle peridotites from the Monte del Estado massif (Southwest Puerto Rico): a preserved section of Proto-Caribbean lithospheric mantle? Geol. Acta 9, 289–306. http://dx.doi.org/10.1344/105.000001713.

Marchesi, C., Garrido, C.J., Proenza, J.A., Hidas, K., Varas-Reus, M.I., Butjosa, L., Lewis, J.F., 2016. Geochemical record of subduction initiation in the sub-arc mantle:

insights from the Loma Caribe peridotite (Dominican Republic). Lithos 252–253, 1–15. http://dx.doi.org/10.1016/j.lithos.2016.02.009.
Müntener, O., Manatschal, G., Desmurs, L., Pettke, T., 2010. Plagioclase peridotites in ocean–continent transitions: refertilized mantle domains generated by melt stagnation in the shallow mantle lithosphere. J. Petrol. 51 (1–2), 255–294. http://dx.doi.org/10.1093/petrology/egp087.
Nickel, K.G., Green, D.H., 1985. Empirical geothermobarometry for garnet peridotites and implications for the nature of the lithosphere, kimberlites and diamonds. Earth Planet. Sci. Lett. 73, 158–170.
Nicolas, A., 1989. Structures of Ophiolites and Dynamics of Oceanic Lithosphere. Kluwer Academic Publishing, Dordrecht.
Nicolas, A., Boudier, F., Idelfonse, B., Ball, E., 2001. Accretion of Oman and United Arab Emirates ophiolite – discussion of a new structural map. Mar. Geophys. Res. 21, 147–179.
Nicolas, A., Boudier, F., 2008. Large shear zones with no relative displacement. Terra Nova 20, 200–205.
Ozawa, K., 1984. Olivine-spinel geospeedometry: analysis of diffusion-controlled Mg–Fe^{2+} exchange. Geochim. Cosmochim. Acta 48, 2597–2611. http://dx.doi.org/10.1016/0016-7037(84)90308-9.
Pallister, J.S., Knight, R.J., 1981. Samail ophiolite plutonic suite: field relations, phase variation, cryptic variation and layering, and a model of a spreading ridge magma chamber. J. Geophys. Res. 86, 2673–2697. http://dx.doi.org/10.1029/JB086iB04p02593.
Pearce, J.A., Alabaster, T., Shelton, A.W., Searle, M.P., 1981. The Oman Ophiolite as a Cretaceous arc-basin complex: evidence and implications. Philos. Trans. R. Soc. 300, 299–317. http://dx.doi.org/10.1098/rsta.1981.0066.
Phipps Morgan, J., Chen, Y.J., 1993. The genesis of oceanic crust: magma injection, hydrothermal circulation, and crustal flow. J. Geophys. Res. 98 (B4), 6283–6297. http://dx.doi.org/10.1029/92JB02650.
Putirka, K.D., 2008. Thermometers and barometers for volcanic systems. Rev. Mineral. Geochem. 69, 61–120. http://dx.doi.org/10.2138/rmg.2008.69.3.
Quick, J.E., Denlinger, R.P., 1993. Ductile deformation and the origin of layered gabbro in ophiolites. J. Geophys. Res. 98 (B8), 14015–14027. http://dx.doi.org/10.1029/93JB00698.
Riches, A.J.V., Rogers, N.W., 2011. Mineralogical and geochemical constraints in the shallow origin, ancient veining, and multi-stage modification of the Lherz peridotite. Geochim. Cosmochim. Acta 75, 6160–6182.
Rioux, M., Bowring, S., Kelemen, P.B., Gordon, S., Dudas, F., Miller, R., 2012. Rapid crustal accretion and magma assimilation in the Oman-U.A.E. ophiolite: high precision U–Pb zircon geochronology of the gabbroic crust. J. Geophys. Res. 117 (B7). http://dx.doi.org/10.1029/2012JB009273.
Rioux, M., Bowring, S., Kelemen, P.B., Gordon, S., Miller, R., Dudas, F., 2013. Tectonic development of the Samail ophiolite: high-precision U–Pb zircon geochronology and Sm–Nd isotopic constraints on crustal growth and emplacement. J. Geophys. Res. 118 (5), 2085–2101. http://dx.doi.org/10.1002/jgrb.50139.
Rioux, M., Garber, J., Bauer, A., Bowring, S., Searle, M., Kelemen, P.B., Hacker, B., 2016. Synchronous formation of the metamorphic sole and igneous crust of the Samail ophiolite: new constraints on the tectonic evolution during ophiolite formation from high-precision U–Pb zircon geochronology. Earth Planet. Sci. Lett. 451. http://dx.doi.org/10.1016/j.epsl.2016.06.051.
Seitz, H.M., Altherr, R., Ludwig, T., 1999. Partitioning of transition elements between orthopyroxene and clinopyroxene in peridotitic and webseritic xenoliths: new empirical geothermometers. Geochim. Cosmochim. Acta 63 (23–24), 3967–3982. http://dx.doi.org/10.1016/S0016-7037(99)00163-5.
Seyler, M., Brunelli, D., Toplis, M.J., Mével, C., 2011. Multiscale chemical heterogeneities beneath the eastern Southwest Indian Ridge (52°E–68°E): trace element compositions of along-axis dredged peridotites. Geochem. Geophys. Geosyst. 12, Q0AC15. http://dx.doi.org/10.1029/2011GC003585.
Sinton, J.M., Detrick, R.S., 1992. Mid-ocean ridge magma chambers. J. Geophys. Res. 97, 197–216. http://dx.doi.org/10.1029/91JB0258.
Sleep, N.H., 1975. Formation of oceanic crust: some thermal constraints. J. Geophys. Res. 80, 4037–4042. http://dx.doi.org/10.1029/JB080i029p04037.
Smith, D., 2013. Olivine thermometry and source constraints for mantle fragments in the Navajo Volcanic Field, Colorado Plateau, southwest United States: implications for the mantle wedge. Geochem. Geophys. Geosyst. 14 (3), 693–711. http://dx.doi.org/10.1002/ggge.20065.
Sun, C., Liang, Y., 2014. An assessment of subsolidus re-equilibration on REE distribution among mantle minerals olivine, orthopyroxene, clinopyroxene, and garnet in peridotites. Chem. Geol. 372, 80–91.
Sun, C., Liang, Y., 2015. A REE-in-garnet–clinopyroxene thermobarometer for eclogites, granulites and garnet peridotites. Chem. Geol. 393–394, 79–92. http://dx.doi.org/10.1016/j.chemgeo.2014.11.014.
Takazawa, E., Okayasu, T., Satoh, K., 2003. Geochemistry and origin of the basal lherzolites from the northern Oman ophiolite (northern Fizh block). Geochem. Geophys. Geosyst. 4 (2), 1021. http://dx.doi.org/10.1029/2001GC000232.
Tilton, G.R., Hopson, C.A., Wright, J.E., 1981. Uranium-lead isotopic ages of the Samail Ophiolite, Oman, with applications to Tethyan ocean ridge tectonics. J. Geophys. Res. 86, 2763–2775. http://dx.doi.org/10.1029/JB086iB04p02763.
Turcotte, D.L., Schubert, G., 2002. Geodynamics, second ed. Cambridge University Press, Cambridge.
VanTongeren, J.A., Kelemen, P.B., Hanghøj, K., 2008. Cooling rates in the lower crust of the Oman ophiolite: Ca in olivine, revisited. Earth Planet. Sci. Lett. 267, 69–82. http://dx.doi.org/10.1016/j.epsl.2007.11.034.
VanTongeren, J.A., Hirth, G., Kelemen, P.B., 2015. Constraints on the accretion of the gabbroic lower oceanic crust from plagioclase lattice preferred orientation in the Samail ophiolite. Earth Planet. Sci. Lett. 427, 249–261. http://dx.doi.org/10.1016/j.epsl.2015.07.001.
Wang, C., Liang, Y., Xu, W., 2015. On the significance of temperature derived from major element and REE based two-pyroxene thermometers for mantle xenoliths from the North China Craton. Lithos 224–225, 101–113. http://dx.doi.org/10.1016/j.lithos.2015.01.022.
Warren, J.M., Shimizu, N., Sakagushi, C., Dick, H.J.B., Nakamura, E., 2009. An assessment of upper mantle heterogeneity based on abyssal peridotite isotopic compositions. J. Geophys. Res. 114. http://dx.doi.org/10.1029/2008JB006186.
Warren, J.M., 2016. Global variations in abyssal peridotite compositions. Lithos 248–251, 193–219. http://dx.doi.org/10.1016/j.lithos.2015.12.023.
Wells, P.R.A., 1977. Pyroxene thermometry in simple and complex systems. Contrib. Mineral. Petrol. 62, 129–139. http://dx.doi.org/10.1007/BF00372872.
Witt-Eickschen, G., Seck, H.A., 1991. Solubility of Ca and Al in orthopyroxene from spinel peridotite: an improved version of an empirical geothermometer. Contrib. Mineral. Petrol. 106, 431–439. http://dx.doi.org/10.1007/BF00321986.
Witt-Eickschen, G., O'Neill, H.S.C., 2005. The effect of temperature on the equilibrium distribution of trace elements between clinopyroxene, orthopyroxene, olivine, and spinel in upper mantle peridotite. Chem. Geol. 221, 65–101. http://dx.doi.org/10.1016/j.chemgeo.2005.04.005.
Wood, B.J., Banno, S., 1973. Garnet–orthopyroxene and orthopyrosene–clinopyroxene relationships in simple and complex systems. Contrib. Mineral. Petrol. 42, 109–124. http://dx.doi.org/10.1007/BF00371501.
Yao, L., Liang, Y., 2015. Closure temperature in cooling bi-mineralic systems: I. Definition and with application to REE-in-two-pyroxene thermometer. Geochim. Cosmochim. Acta 162, 137–150. http://dx.doi.org/10.1016/j.gca.2015.03.041.